Author Manuscript

Author Manuscript

Author Manuscript

Author Manuscript

HHS Public Access

Author manuscript

Neuron. Author manuscript; available in PMC 2016 May 20.

Published in final edited form as:

Neuron. 2015 May 20; 86(4): 923–935. doi:10.1016/j.neuron.2015.03.066.

Spatiotemporal control of opioid signaling and behavior

Edward R. Siuda[1,4,6], **Bryan A. Copits**[1,2,6], **Martin J. Schmidt**[1,6], **Madison A. Baird**[1,6], **Ream Al-Hasani**[1], **William J. Planer**[1], **Samuel C. Funderburk**[1], **Jordan G. McCall**[1,4], **Robert W. Gereau IV**[1,2,3,4], and **Michael R. Bruchas**[1,2,3,4,5]

[1]Department of Anesthesiology, Basic Research Division, Washington University in St. Louis, St. Louis, MO, 63110, USA

[2]Washington University Pain Center, Washington University in St. Louis, St. Louis, MO, 63110, USA

[3]Department of Anatomy and Neurobiology, Washington University in St. Louis, St. Louis, MO, 63110, USA

[4]Division of Biological and Biomedical Sciences, Washington University School of Medicine, Washington University School of Medicine, St. Louis, MO 63110

[5]Department of Biomedical Engineering, Washington University in St. Louis, St. Louis, MO 63110

Summary

Optogenetics is now a widely accepted tool for spatiotemporal manipulation of neuronal activity. However, a majority of optogenetic approaches use binary on/off control schemes. Here we extend the optogenetic toolset by developing a neuromodulatory approach using a rationale-based design to generate a Gi-coupled, optically-sensitive, mu-opioid-like receptor, we term opto-MOR. We demonstrate that opto-MOR engages canonical mu-opioid signaling through inhibition of adenylyl cyclase, activation of MAPK and G protein-gated inward rectifying potassium (GIRK) channels, and internalizes with similar kinetics as the mu-opioid receptor. To assess *in vivo* utility we expressed a Cre-dependent viral opto-MOR in RMTg/VTA GABAergic neurons, which led to a real-time place preference. In contrast, expression of opto-MOR in GABAergic neurons of the ventral pallidum hedonic cold spot, led to real-time place aversion. This tool has generalizable application for spatiotemporal control of opioid signaling and, furthermore, can be used broadly for mimicking endogenous neuronal inhibition pathways.

© 2015 Published by Elsevier Inc.

Address correspondence to: Michael R. Bruchas, PhD: bruchasm@wustl.edu.

[6]These authors contributed equally to this work

MAB current address: University of Washington, Department of Pharmacology, Seattle, WA

Publisher's Disclaimer: This is a PDF file of an unedited manuscript that has been accepted for publication. As a service to our customers we are providing this early version of the manuscript. The manuscript will undergo copyediting, typesetting, and review of the resulting proof before it is published in its final citable form. Please note that during the production process errors may be discovered which could affect the content, and all legal disclaimers that apply to the journal pertain.

Author Contributions

ERS, BAC and MJS designed and performed experiments, collected and analyzed data and wrote the manuscript. MAB, RA, SCF, JGM designed and performed experiments, collected and analyzed data. WJP provided technical support and facilitated design, construction, and cloning of the receptor chimera and virus. RWG helped design and oversee experiments. MRB helped design, analyze, and oversee experiments, and wrote the manuscript.

Author Manuscript Author Manuscript Author Manuscript Author Manuscript

Keywords

optogenetics; opto-XR; GPCR; opioid; mu-opioid receptor; reward; aversion; ventral tegmental area; ventral pallidum; periaqueductal gray; GIRK; pain

Introduction

Opioid receptor targeting drugs have been used as analgesics and recreationally abused for hundreds of years. Due to a lack of effective alternatives, they remain on the front lines for acute pain management, severe anti-tussive treatment, and other indications despite their high abuse potential. Mu (MOPR), kappa (KOPR), delta (DOPR), and nociceptin receptors (NOPR) persist at the forefront of basic science and drug discovery efforts on disorders ranging from gastrointestinal ailments to pain, addiction, and depression (Al-Hasani and Bruchas, 2011). Among these receptor systems, the mu opioid receptor has been the most intensely studied due to its long-established involvement in analgesia, euphoria, and reward in response to morphine-like analogues. However, despite years of study, opioid research had been limited by a fundamental challenge. Studying the specific effects of opioids with spatial, temporal, and cell-type specific control is virtually untenable, especially in the context of the central nervous system. Systemic drugs bind MOPRs on heterogeneous cell populations across multiple brain regions. MOPR expression at both pre- and post-synaptic sites within overlapping discrete regions precludes determination of circuit level contributions. Therefore, approaches to selectively limit engagement of MOPR signaling to restricted cell populations with temporal control that closely mimics endogenous opioid kinetics is a first key step towards unraveling these issues and for developing future therapeutic strategies where opioids are the most effective treatment regimen.

Recent developments in optogenetics and molecular biology provide an ideal strategy for addressing these questions. Class A G-protein coupled receptors (GPCRs), including the rat rhodopsin receptor and MOPR, have structural and functional similarities that can be exploited to create hybrid receptors with unique functional properties. More specifically, the light-sensitive external portion of rhodopsin receptors can be combined with internal signal transduction components of other GPCRs to produce so-called optoXR chimeras capable of initiating and terminating receptor-specific signaling events with the temporal precision enabled by pulses of light (Airan et al., 2009; Gunaydin et al., 2014; Kim et al., 2005; Masseck et al., 2014). Furthermore, packaging these receptors into Cre recombinase-dependent viruses using loxP flanked doubled inverted open (DIO or FLEX) reading frames allows for restricted expression in discrete cell types within isolated brain regions yielding spatial control of GPCR signaling *in vivo* (Atasoy et al., 2008; Zhang et al., 2010).

Here, we present the generation and characterization of a new photosensitive mu-opioid-like chimeric receptor (we term opto-MOR). We show that opto-MOR suppresses cAMP levels, activates MAPK signaling, and internalizes in a similar time course to native MOPR. Furthermore, it functionally couples to GIRK channels in GABAergic neurons of the periaqueductal gray (PAG) and rostromedial tegmental region (RMTg), mimicking properties of native MOPR (Blanchet and Lüscher, 2002; Ingram et al., 2008; Matsui et al.,

Author Manuscript Author Manuscript Author Manuscript Author Manuscript

2014; Vaughan et al., 2003). Finally, we demonstrate here that opto-MOR promotes classical MOPR-mediated reward and aversion behaviors in distinct brain circuits. Together these findings establish opto-MOR as a spatiotemporally precise MOPR analogue and support its utility for studying opioid circuitry and behavior.

Results

Developing a chimeric photosensitive receptor with components of the mu opioid receptor

In order to effectively generate an optically-sensitive MOPR-based receptor chimera that would have high probability of structural similarity to mu-opioid receptors and retain native opioid Gi/o-protein signaling we used the closest class A-related receptor as a backbone. Rat rhodopsin RO4 has been previously shown to couple to Gi/o signaling pathways *in vitro*, and thus served as the ideal template for generation of an opto-MOR (Hille, 1994). Using the constraint-based multiple alignment tool (COBALT, NCBI; http://www.st-va.ncbi.nlm.nih.gov/tools/cobalt/re_cobalt.cgi), rat rhodopsin RO4, was aligned against rat MOPR to identify and align transmembrane, intracellular, and extracellular domains (Figures 1A and S1A). To confer MOPR-like coupling, we isolated the rhodopsin RO4 sequence, retained the critical photoisomerizing RO4 retinal binding site (Figures S1A and S1B) and inserted the rat MOPR intracellular loops and C-terminus (Figures S1A and S1C). A protein folding prediction was modeled by bioinformatics software (Roy et al., 2010) in order to accurately project how our various chimeras would result in a seven transmembrane protein with matched features (Figures 1A and S1D). This approach allowed for optimal conservation of Gi/o receptor dynamics, a high degree of photosensitivity, while simultaneously providing the critical intracellular communication components for engaging mu-opioid signaling pathways *in vitro* and *in vivo*.

Opto-MOR is photosensitive and effectively mimics mu-opioid signaling dynamics

In order to determine if opto-MOR is functional and traffics to the membrane we first examined whether a YFP-tagged opto-MOR expresses at the cell membrane in a similar pattern to the wild type MOPR-GFP tagged receptor. We found that both receptors express at the plasma membrane in a similar manner (Figures 1B and 1C) in unstimulated cells. Opioid receptor characterization has demonstrated that agonist stimulation of opioid receptors causes interactions with inhibitory G-proteins (Gαi) to induce inhibition of cAMP production (Childers and Snyder, 1978; Al-Hasani and Bruchas, 2011) (Figure 1A). In order to determine whether cells expressing opto-MOR couple to the same canonical MOPR signaling pathways, we assessed their response to blue LED (465 nm, 1 mW, 20 sec) stimulation in a battery of well-known *in vitro* opioid signaling assays in direct parallel with wild-type rat MOPR using the high affinity, selective MOPR agonist, D-Ala^2, NMe-Phe^4, Gly-ol^5]-enkephalin (DAMGO; 1 μM). First, we show that opto-MOR maintains similar membrane expression levels as MOPR in unstimulated HEK293 cells (Figures 1B and 1C). Second, we found that photostimulation of opto-MOR and DAMGO activation of MOPR caused a time-locked decrease in forskolin-induced intracellular cAMP levels with similar time constants of activation (Figures 1D–F, S2A,B and S2D,E). To verify the specificity of our constructs, we show that opto-MOR does not respond to the selective MOPR full agonist DAMGO, and likewise wild-type MOPR does not respond to photostimulation (Figures S2C

Author Manuscript Author Manuscript Author Manuscript Author Manuscript

and S2F). Additionally, we show that opto-MOR is maximally activated with 465 nm light and shows less efficacy at other wavelengths in cAMP inhibition (525, 630, and 660 nm) (Figure 1G). Finally, we found that opto-MOR is highly sensitive to light and requires very little light power for photoactivation (Figures 1H and S2G), while varying LED pulse lengths resulted in similar levels of cAMP inhibition (Figure 1I). Opto-MOR and MOPR caused similar levels of cyclic AMP inhibition via photostimulation and agonist treatment, respectively, suggesting that opto-MOR couples to canonical mu-opioid signaling pathways, yet utilizes rapid time-locked photoswitching to engage Gαi-mediated inhibition of adenylyl cyclase signaling.

Agonist stimulation of all four opioid receptors has been shown to recruit various factors resulting in mitogen activated protein kinase (MAPK) activation (Bruchas et al., 2011; Al-Hasani and Bruchas, 2011). MOPR has been shown to elicit a rapid initial peak in the phosphorylation of extracellular signaling-regulated kinase (pERK) in neurons, astrocytes and transfected cell cultures (Belcheva et al., 2005). Here we examined whether opto-MOR and MOPR produce similar kinetics and efficacy in engaging pERK signaling in HEK293 cells. In complementary experiments, we found a rapid and transient increase in pERK (~2–5 min) in response to blue LED photostimulation of opto- MOR and DAMGO application to MOPR expressing cells (Figures 1J–L). pERK returned to basal levels 60–90 min after either photostimulation or DAMGO treatment. Furthermore, opto-MOR-mediated activation of ERK was mostly independent of LED pulse time (Figure S2H) and only mildly affected by light power (Figure S2I), suggesting that time locked photoactivation of opto-MOR immediately engages the MAPK signaling cascade.

Opioid receptors are well known to be rapidly regulated by arrestin-clathrin mediated internalization pathways. To assess whether opto-MOR exhibits similar activation-induced receptor regulation and engages canonical mu-opioid receptor internalization machinery, we performed side-by-side experiments whereby we compared the kinetics and efficacy of LED or agonist stimulated receptor internalization on opto-MOR or MOPR. Following photostimulation or DAMGO treatment, respectively, both opto-MOR and MOPR internalized rapidly (within 15 min) with similar rates of internalization (τ_{in}), with a peak effect at 30 min after agonist or light stimulation (Figures 2A,B and S3A,B). Opto-MOR receptors remained punctate in the cytosol at all post stimulation times tested, lasting up to an hour. Opto-MOR internalization over this time course is consistent with previously reported wild-type MOPR internalization by both widely used synthetic and endogenous ligands.

Agonists such as etorphine, DAMGO and endogenous opiate peptides such as Met-enkephalin and β-endorphin have been shown to cause MOPR internalization 30 minutes after drug exposure, as receptor endocytosis and recycling to the membrane reaches steady state around 30 and 60 minutes, respectively. To test whether opto-MOR displays functional desensitization in addition to internalization, we photostimulated opto-MOR and induced inhibition of cAMP (Figures 2C and 2F). In parallel, we photostimulated opto-MOR expressing HEK293 cells at saturating power (1 mW, 20 sec) waited varying degrees of time, and then photostimulated again (*i.e*. pre-pulsed). We found that at approximately 15 min following pre-pulse stimulation, there is a significant loss of opto-MOR function, with

Author Manuscript Author Manuscript Author Manuscript Author Manuscript

no difference observed from the unstimulated control cells (Figures 2D and 2F). However, longer time periods between the two light pulses show that within approximately 60 min, there is restoration of opto-MOR function in inhibition of cAMP (Figures 2E and 2F). However, it is unclear whether this restoration is due to receptor recycling or *de novo* receptor synthesis. To address this, we repeated this experiment but pretreated cells with either brefeldin A, which blocks translocation of proteins from the endoplasmic reticulum to the Golgi, and has been used in studies of MOPR recycling, or Dyngo-4a, an inhibitor of dynamin that prohibits receptor internalization, and has recently been shown to prevent intracellular GPCR cAMP signaling. Following a 1 hour interpulse interval (Figure S3D), we found that pretreatment with brefeldin A did not prevent opto-MOR-induced inhibition of cAMP (Figure S3C and S3E). Furthermore, Dyngo-4a pretreated cells also show cAMP inhibition suggesting that opto-MOR continues to inhibit cAMP from the plasma membrane with no loss of signal when inhibiting dynamin-clathrin pathways (Figure S3C and S3F). These data together suggest that opto-MOR may indeed recycle and use clathrin-dynamin endocytosis which has been documented in opioid receptors (Gupta et al., 2014) and other GPCR systems (Irannejad et al., 2013; Tsvetanova and von Zastrow, 2014), and suggests that opto-MOR may have some utility in dissecting these diverse signaling dynamics.

Opto-MOR expresses and is a functional receptor in DRG neurons

To test whether opto-MOR is expressed and functions outside the context of an artificial heterologous system, we generated a Cre-dependent adeno-associated viral construct (Figure 3A), whereby we inserted opto-MOR into a double inverted open-reading frame flanked by LoxP and Lox2227 sites (Zhang et al., 2010). Utilizing this virus (AAV5-EF1α-DIO-opto-MOR-YFP) we infected cultured dorsal root ganglia (DRG) neurons from Advillin-Cre^{+} mice (da Silva et al., 2011; Zhou et al., 2010). We did not detect any signal in uninfected control neurons (Figure 3B). In Advillin-IRES-Cre+$^{\text{opto-MOR}}$ DRG neurons, we observed opto-MOR expression in as little as 2 days post-transduction (green, Figure 3C), suggesting rapid Cre-mediated excision in DRG. Strong opto-MOR expression was seen after 5 days (Figure 3D), which partially co-localized with synapsin (Figure 3D) demonstrating that opto-MOR is trafficked efficiently along neuronal processes and to presynaptic terminals. We also show that following photostimulation of opto-MOR expressing DRGs, there is an increase in pERK compared to untreated controls (Figures 3E and 3H). Following photostimulation (1 min, 1 mW) we observed an increase in pERK levels 5 min following an initial light stimulation that returns to basal levels within 30 min (Figures 3F–H). We also report evidence for photostimulated receptor internalization in these DRG cultures (Figure 3F–H) suggesting that the receptor can be dynamically regulated in physiological relevant systems. These data closely mimic the kinetics of ERK activation seen in HEK293 cells expressing opto-MOR (Figures 1J,K) and further support the utility of using opto-MOR to dissect signaling in neuronal preparations.

Opto-MOR couples to Gβγ -mediated GIRK currents in PAG GABAergic neurons

In order to assess whether opto-MOR couples to similar intracellular signaling pathways following endogenous MOPR activation in neurons, we focused on the periaqueductal gray (PAG), which contains a high proportion of MOPR^{+} neurons (Vaughan et al., 2003). We injected AAV5-EF1α-DIO-opto-MOR-YFP into vGAT-IRES-Cre^{+} mice (Vong et al., 2011)

Author Manuscript Author Manuscript Author Manuscript Author Manuscript

within the periaqueductal gray (PAG) (AP: −5.0 mm, ML: +/− 0.5 mm, DV: −2.8 mm) and targeted YFP^+ GABAergic neurons for whole-cell recordings from acute brain slices 2–3 weeks after injection. Photostimulation with 470 nm LED light (10 mW/mm^2) evoked rapid outward currents together with a simultaneous decrease in input resistance that was reversed by bath application of barium (1 mM), a blocker of GIRK currents (Figures 4A and 4B), suggesting opto-MOR activation leads to downstream activation of GIRK channels, which is consistent with the activation of endogenous MOPR receptors in these neurons (Vaughan et al., 2003). A parallel set of experiments was performed on MOPR positive cells in the PAG. Bath application of DAMGO (1 μM) showed similar outward currents and decreased input resistance that were also barium sensitive (Figures 4C and 4D). Voltage ramps performed pre- and post-stimulation demonstrated current-voltage curves consistent with the properties of GIRK channels, which were inhibited by barium (Figure 4G, and 4H). Peak changes in holding current and input resistance for opto-MOR (LED) and MOPR (DAMGO) were not statistically different following stimulation, or in the presence of barium (Figures 4E and 4F), suggesting that activation of both receptors is coupled to similar downstream effectors. We also found that activation of both opto-MOR and MOPR substantially decreased neuronal excitability in response to step current injections, which was also reversed by application of barium (Figures 4I and 4J). We did however, noticed a persistent outward current and significantly reduced input resistance following washout of barium (Figures 4K and 4L) indicating that brief activation of opto-MOR can couple to downstream effectors to suppress neuronal activity for an extended period of time.

We next asked whether opto-MOR and MOPR activation engages converging intracellular signaling cascades leading to GIRK channel activation, or whether these two receptor populations signal through parallel subcellular pathways. To test this, we recorded from $MOPR^+/YFP^+$ GABAergic neurons in the PAG and applied saturating concentrations of DAMGO (1 μM). We observed sustained outward currents coupled with a decrease in input resistance (Figure 5A). After this response plateaued, we stimulated neurons with either a brief LED light pulse (5 sec, Figure 5A) or prolonged illumination (1 min, Figure 5B and 5C). We found that opto-MOR coupling to GIRK channel currents and changes in input resistance were occluded by sustained activation of endogenous mu-opioid receptors (Figures 5D–5F), suggesting that activation of opto-MORs converge onto the same pool of intracellular signaling cascades as endogenous mu opioid receptors. In addition, we injected AAV5-EF1α-DIO-opto-MOR-YFP into the rostral tegmental nucleus (RMTg) (AP: −3.9 mm, ML: −0.1 mm, DV: −4.5 mm) of a new cohort of vGAT-IRES-Cre mice and targeted YFP^+ interneurons for whole-cell recordings. Photostimulation with 470 nm LED light (10 mW/mm^2) evoked outward currents together with a decrease in the input resistance (Figure S4A and S4B), suggesting opto-MOR activation is coupled to GIRK channels, which is consistent with the endogenous MOPR function in these neurons (Matsui and Williams, 2011; Matsui et al., 2014). Voltage ramps performed pre- and post-stimulation demonstrated current-voltage curves consistent with the properties of GIRK channels (Lüscher et al., 1997) (Figure S4C).

Taken together, these results from two different brain regions suggest that opto-MOR couples to canonical MOPR G-protein signaling pathways, yet retains rapid photo-

Author Manuscript Author Manuscript Author Manuscript Author Manuscript

engagement of opioid signal transduction pathways, making it an ideal tool for spatiotemporal approaches to study MOPR signaling in real time *in vivo*.

In vivo photostimulation of opto-MOR in selected GABAergic neurons mediates preference or aversion

To demonstrate the utility of opto-MOR for studying opioid neural circuits in behavior, we locally infused AAV5-EF1α-DIO-opto-MOR-YFP into the brains of two naïve groups of vGAT-IRES-Cre mice; one group in the RMTg (Figure 6A) and one group in the ventral pallidum (VP) (Figure 6B), and waited at least three weeks for optimal viral expression at the soma (Figures 6C,D and 6E,F). Fiber optic implants (Sparta et al., 2012) were chronically implanted above the VTA and the VP respectively. Mice were placed into black opaque boxes and allowed to explore both chambers freely to evaluate preference or aversion behavior using the real time place preference assay. During testing, mice received constant 10 mW 473 nm blue laser light upon entry into the "light stimulation" side (Figures 6G and 6I). Preference and aversion were calculated as the difference in time spent in the light stimulated box compared to the box with no stimulation with preference defined as more time spent in the photostimulated box and aversion defined as less time in the photostimulation chamber. vGAT-IRES-Cre+$^{\text{opto-MOR:RMTg}}$ mice displayed a significantly greater preference for the stimulation than their Cre(−) injected opto-MOR littermate controls (Figures 6G,H; $t_{13}=2.231$, $p<0.05$; and Figures S5A and S5B). In addition, based on our data demonstrating a power response relationship with opto-MOR in activating cAMP and pERK (Figures 1H and S2I), we posited that different light powers might produce different behavioral phenotypes. As such, we focused on real time place preference in vGAT-IRES-Cre+$^{\text{opto-MOR:RMTg}}$ mice. We found that animals receiving no light stimulation in the VTA show no preference for either chamber (Figure S5I). However, when we increase the power to 1 mW, animals begin to show a place preference and spend more time in the conditioned chamber than those receiving no light stimulation, but less time than those receiving 10 mW photostimulation (Figure S5I), thus demonstrating that opto-MOR signaling can be more finely manipulated *in vivo*.

In contrast, mice injected with opto-MOR into the VP (vGAT-IRES-Cre+$^{\text{opto-MOR:VP}}$) displayed significant place aversion to photostimulation, as compared to Cre(−) littermate controls (Figures 6I and 6J; $t_{19}=2.174$, $p<0.05$; and S5E and S5F). Importantly, there were no differences in locomotor activity throughout the session for either group (Figures S5C and S5G) and light stimulation did not induce acute changes in locomotion in the stimulation chamber (Figures S5D and S5H). Finally as a positive control, and to compare the efficacy of our opto-MOR experiments for a more traditional optogenetic strategy, we tested a new cohort of mice in which we inhibited GABAergic neurons in the VTA using halorhodopsin (NpH3.0) in the real time preference assay (Figures S5J–L) as previously reported (Jennings et al., 2013). These data were strikingly similar to inhibiting RMTg GABAergic neuronal population with opto-MOR (Figure S5A) suggesting that inhibition of these populations has comparable behavioral phenotypes with alternative optogenetic tools. Taken together, these behavioral results indicate that opto-MOR functions to engage signaling and neuronal inhibition with the ability to elicit robust real time behavioral responses.

Author Manuscript Author Manuscript Author Manuscript Author Manuscript

Discussion

Here we describe the development of a new opto-XR receptor based on the mu-opioid receptor. We show that this opto-MOR behaves functionally like its wild type MOR counterpart in engaging canonical opioid G-protein signaling pathways and receptor internalization. Furthermore, we found that selective expression of opto-MOR in GABAergic neurons within two distinct brain regions promotes diverse behavioral responses consistent to those previously observed with local MOPR agonist infusion. This opto-MOR receptor could potentially also be used alongside chemogenetic approaches, in peripheral studies to assess nociceptive circuits, or as a robust way to inhibit neuronal activity without the limits of the currently used Cl^- and H^+ pump approaches that include halorhodopsin or archaerhodopsin (Berndt et al., 2014; Raimondo et al., 2012; Wietek et al., 2014).

Opto-MOR mimics mu-opioid receptor signaling *in vitro*

A few other opto-XR receptors have been reported (Airan et al., 2009; Barish et al., 2013; Kim et al., 2005) including an opto-β_2 adrenergic receptor as well as the recently described 5HT1A-like opsin-chimera using the c-terminal components of the wild-type receptor (Masseck et al., 2014). However, few reports have directly examined the intracellular signaling dynamics of opto-XR signaling as they relate to their wild type receptor counterpart, nor have these receptors been utilized in native circuits where their endogenous complementary receptor types are expressed. This report shows side-by-side that GPCR Class A rhodopsin-like chimeras can be generated to mimic neuropeptide receptor function *in vitro*. We found that opto-MOR indeed engages inhibition of cAMP, couples to GIRK outward currents in neurons, and activates ERK rapidly following light pulse exposure (within 2 min), and finally that opto-MOR internalizes rapidly in response to photostimulation. Furthermore, we show the opto-MOR receptors functionally desensitize (Figures 2A,B), in a similar manner to their wild-type MOPR counterparts, suggesting that these receptors couple to native downregulation signaling pathways including G protein-coupled receptor kinases (GRKs), and arrestins. In addition, our data suggest that similar to other previously reported GPCRs, these receptors may potentially signal at both membrane and intracellular domains (Irannejad et al., 2013). The possibility therefore exists that opto-MOR may be capable of optical activation while localized intracellularly, highlighting not only an important caveat, but also illustrating the potential utility of this chimera to elucidate components of intracellular signaling cascades. However, future studies to examine opto-MOR regulation of signaling dynamics in native neurons are required, and mutation of the opto-MOR receptor at c-terminal cites previously associated with receptor regulation could potentially provide advantageous optogenetic tools in dissecting MOPR-related signaling and tolerance *in vivo*.

In vivo utility of Opto-MOR for behavioral optogenetic studies

We primarily generated this unique tool to facilitate mimicry of opioid signaling *in vivo* for use in optogenetic studies. The ability to time-lock activation of mu-opioid-like signaling in an awake-behaving animal provides an alternate approach for mapping the role of opioid receptor signaling in discrete neural circuits and cell populations in real time. In order to

Author Manuscript Author Manuscript Author Manuscript Author Manuscript

demonstrate the utility of this approach *in vivo* we chose two brain regions widely known to express high levels of endogenous MOPR that have previously been linked to mu-opioid dependent reward and aversion. In a first series of experiments we examined the effects of opto-MOR expression in VTA/RMTg GABAergic neurons using real time place testing. Recent work had demonstrated that mu-opioid receptors are expressed on both local VTA interneurons as well as a large proportion of nearby RMTg GABAergic cells. It is hypothesized that these receptors likely act to disinhibit dopaminergic activity resulting in MOPR-mediated reward behavior. We demonstrate here that photostimulation of opto-$MOR^{VGATcre+}$ receptors in RMTg neurons produces real time place preference, and reward seeking behavior. This result is consistent with reports using mu opioid agonists into this region (Jalabert et al., 2011; Jhou et al., 2012; Matsui et al., 2014). In addition, prior reports have demonstrated that optogenetic activation or inhibition of VTA and RMTg GABAergic neurons drives real time place preference or aversion behavior (Tan et al., 2012; van Zessen et al., 2012), further suggesting that these VTA neuronal populations are poised to regulate dopaminergic output and behavior.

The ventral pallidum (VP) region is well known to express mu-opioid receptors and regional activation has been reported to lead to both reward and aversive behavioral responses (Hjelmstad et al., 2013). We therefore expressed opto-MOR in VP GABAergic neurons and selectively targeted coordinates corresponding to the previously reported opioid “hedonic cold spot,” (Smith and Berridge, 2005; Smith et al., 2009) in order to determine if activation of opto-MOR signaling in this region could elicit real time aversion. Consistent with prior reports showing that MOPR agonism in this anterior central region decreases reward seeking (Smith et al., 2009), we observed that opto-MOR activation within these neurons produced avoidance of the photostimulation chamber. These two behavioral assays demonstrate that opto-MOR can elicit robust real time opioid-like behavioral responses *in vivo*, and highlight their utility for future studies examining circuit and cell-type functions of this pathway.

In addition, these *in vitro* and *in vivo* findings coupled with our evidence of coupling to GIRK signaling highlight the utility of opto-MOR for more generalizable optogenetic inhibition studies, such as those that are routinely conducted using halorhodopsin or archaerhodopsin. Opto-MOR couples to native signaling pathways to regulate neuronal activity via GIRKs, and might be preferred since it does not come with the potential caveats that the photosensitive chloride pumps (eNpHR3.0) bring with them including alterations in the reversal potential of the $GABA_A$ receptor that lead to changes in synaptically evoked spiking activity in the period after photoactivation (Raimondo et al., 2012). Future work utilizing opto-MOR in other neuronal cell types and circuits is warranted however, for determining its utility as a broadly generalizable optogenetic inhibition approach.

Limitations and Future Directions

Although we have developed a photosensitive mu-opioid-like receptor for the interrogation of opioid neural circuits *in vitro* and *in vivo*, there are some potential limitations of this approach that are worth noting. We chose to use vertebrate rhodopsin as a backbone for generation of opto-MOR because it has previously been shown to couple to Gi/o-related signaling (Li et al., 2005), and thus made for an ideal chimeric approach. However, this

Author Manuscript Author Manuscript Author Manuscript Author Manuscript

choice of rhodopsin has limitations since the receptor is very photosensitive, as indicated in our *in vitro* studies and *in vivo* behavior. This is an important consideration when using the tool *in vitro* for slice physiology and circuit analysis, as well as *in vivo*, when wanting to elicit discrete activation in a particular anatomic subregion. To work around these caveats we were careful to use the tool under red light conditions *in vitro*, and while *in vivo* we kept the fiber implants capped. To resolve this, future variants might be warranted with mutations that render opto-MOR less photosensitive and/or use other short wavelength opsins as part of the chimeric design.

It is also important to note that the receptor is only partially a mu-opioid receptor, and thus might display a different protein-interactome than the wild-type MOPR. Indeed, we show that the receptor utilizes a similar pool of intracellular signaling as MOPR (Figure 1 and Figure 2), and traffics to synapses (Figure 3), however recent work has suggested a complex regulatory proteome of MOPR interactions (Al-Hasani and Bruchas, 2011), and thus we are careful to interpret our data in light of known transmembrane and extracellular loop residues that are important for MOPR function in neurons.

Future studies using the opto-MOR in side-by-side experiments with other exciting recent developments (Banghart and Sabatini, 2012) in optical control of neuropeptide function should provide researchers with a means to better dissect the role of opioid neuropeptide signaling in complex neural circuits, and in freely moving mice (Kim et al., 2013). Understanding the relative dynamics of neuropeptide release and receptor signaling is a key question in neuroscience, and opto-XRs that mimic endogenous signaling pathways hold promise in delineating some of these mechanisms. Furthermore, there is a growing need to better understand the molecular-cellular mechanisms of opioid tolerance in pain and thus the optodynamic properties of this approach may have utility in this arena. The use of this tool will provide an additional layer of spatiotemporal specificity when used with traditional pharmacology, physiology, and behavioral approaches.

Conclusions

In summary, here we provide and characterize a novel tool for neuroscience that allows for spatiotemporal control of opioid receptor signaling *in vitro* and *in vivo*. Opto-MORs functionally couple to canonical intracellular signaling pathways, and have utility in dissecting opioid contributions to behavioral affect. The combination of opto-XR approaches with chemogenetic and traditional optogenetic channel approaches expands our toolbox for understanding neuropeptide signaling within neural circuits, within real time, freely moving animals. Furthermore, advances in receptor chimeras such as opto-MOR will facilitate the generation of additional related approaches for other GPCR classes.

Experimental Procedures

Construct Design and Cloning

Using the constraint-based multiple alignment tool (COBALT, NCBI; http://www.st-va.ncbi.nlm.nih.gov/tools/cobalt/re_cobalt.cgi), rat rhodopsin 4 (RO4) sequences were aligned against rat MOR. RO4 extracellular domains, including the retinal binding site, and

Author Manuscript Author Manuscript Author Manuscript Author Manuscript

transmembrane domains were identified and conserved. HindIII/EcoRI sites were added to the N-terminus while XhoI/BamHI sites were added to the C-terminus of the chimeric sequence. The stop codons were replaced with leucine residues and silent mutations were added to remove an endogenous XhoI restriction digest site 990bp into the gene. The construct was synthesized by IDT in a non-expressing pSMART vector (Lucigen, Middleton, WI), then cloned without stop codons into pcDNA3-YFP (Invitrogen, Carlsbad, CA) containing ampicillin resistance cassettes and CMV promoter regions for expression in mammalian cells. Restriction enzyme digest sites EcoRI and XhoI were used to excise the opto-receptor construct from the pSMART vector and purified by gel extraction. pcDNA3-YFP was also digested with EcoRI and XhoI and T4 Ligase were used to ligate opto-MOR into the vector. *E. Coli* was transformed with pcDNA3-opto-MOR-YFP plasmids, plated on ampicillin containing plates. GeneWiz (South Plainfield, NJ) verified chimeric sequence integrity. Rat MOR-GFP was kindly donated from the lab of Dr. Charles Chavkin at University of Washington, Department of Pharmacology (Celver et al., 2004).

Real-time measurement of cAMP dynamics

Stable HEK cell lines containing opto-MOR and MOR were transfected with the pGloSensor-22F cAMP plasmid (Promega E2301) using JetPrime (Polyplus) transfection reagent per manufacturer's instructions. Stable co-transfected cells were maintained under both G418 (400 μg/ml) and hygromycin (200 μg/ml) selective pressure. The day before an experiment, cells were plated on 96-well tissue culture treated plates (Costar), 60–100K cells/well, and allowed to recover overnight at 37°C, 5% CO_2. The next day, media was replaced with 2% GloSensor reagent (Promega) suspended in CO_2-independent growth medium (Gibco) and incubated for 2 hours at 37°C. For real time cAMP, a baseline was first obtained with no treatment by recording relative luminescent units (RLUs) every 6 sec for 1 min using a SynergyMx microplate reader (BioTek; Winooski VT; USA). 1 μM forskolin (dashed line in each figure) was applied to each well and RLUs recorded for 3 min. Cells were then treated with either a 20 sec, 1 mW, blue LED pulse or 1 μM DAMGO (Tocris) and RLUs recorded for an additional 10 min. For data expressed as cAMP (fold baseline), RLUs for 1 min of baseline were averaged and all subsequent RLUs were then divided by this average. For data expressed as cAMP (% max), raw RLUs were entered into GraphPad Prism (v5.0d, GraphPad Software, San Diego California USA) and the normalization function used to assign the lowest RLU a value of 0% and the highest RLU a value of 100%. Time constants were calculated in GraphPad Prism using one-phase association (Y=Y0 + (Plateau-Y0)*(1-exp(-K*x))) nonlinear regression analyses yielding a time constant value (τ_{on}). For cAMP (% control) data, area under the curve for each treatment group was normalized to its corresponding experimental control. Each data point is a minimum of 3 wells per experimental replicate.

Immunoblotting

Immunoblotting for MAPK activation was performed as previously described (Bruchas et al., 2011). Opto-MOR and MOPR expressing cells were grown to 100% confluency in 24 well plates. Cells were serum-starved in plain DMEM for at least 4 hours before drug or LED treatment using Plexon LED Driver LD-1 (465 nm). Cells were harvested in 500 μl of lysis buffer containing in mM (50 Tris-HCl, 300 NaCl, 1 EDTA, 1 Na_3VO_4, 1 NaF, 10%

Author Manuscript Author Manuscript Author Manuscript Author Manuscript

glycerol, 1% Nonidet P-40, 1:100 of phosphatase and protease inhibitor mixture set (Calbiochem, EMD Millipore, Darmstadt, Germany). Lysates were sonicated for 10 s and spun down for 20 min (14,000 × g, 4°C). 25 μg protein was run in each well and blots transferred to nitrocellulose (Whatman, Middlesex, UK), blocked with 5% fetal bovine serum albumen for 1 hr, then incubated with 1:1000 goat anti-rabbit pERK1/2 (phospho Thr-202/ Tyr-204; Cell Signaling, Danvers, MA) and 1:20,000 goat anti-mouse β-actin (Abcam, Cambridge, MA) antibodies at 4°C overnight. Membranes were washed 4× for 10 min each in Tris-buffered saline and 0.1% Tween-20 (TBST) and incubated with 1:10,000 IRDyeTM 800- and 700-conjugated affinity purified anti-rabbit or anti-mouse IgG in a 1:1 mixture of 5% milk/TBS and Li-Cor blocking buffer (Li-Cor Biosciences, Lincoln, NE) for 1 hr at room temperature. Membranes were washed 4× for 10 minutes each with TBST then 2× with TBS to remove Tween. Blots were visualized, background subtracted, and quantified with Odyssey Infrared Imager (Li-Cor Biosciences, Lincoln, NE). pERK bands were normalized to β-actin from each sample and calculated as fold increase from baseline or as percent of maximal ERK phosphorylation as appropriate.

Receptor Internalization and Confocal Microscopy

Opto-MOR-YFP and MOPR-GFP expressing cells were plated to approximately 50% confluence on poly-D-lysine-coated coverslips (Becton Dickinson, Franklin Lakes, NJ). Following LED (1 W/cm^2, 1 min) or DAMGO (1 μM) treatment cells were washed 3 times with PBS, and then fixed with 4% paraformaldehyde. Coverslips were then mounted with Vectashield Hard Set mounting medium with DAPI (Vector Laboratories, Burlingame, CA) and imaged on a Leica TCS SPE confocal microscope (Leica, Buffalo Grove, IL) and Application Suite Advanced Fluorescence (LAS AF) software calculated receptor internalization (inside fluorescence/total fluorescence × 100).

Animal subjects

Group-housed adult (25–35 g) male vGAT-IRES-Cre mice (Vong et al., 2011) and Cre(−) littermate controls were used for all *in vivo* experiments. For eNpH3.0 VTA GABA experiments (see supplemental materials), GAD2-Cre mice were used. All mice were maintained on a 12 hr light: 12 hr dark cycle and given *ad libitum* access to food and water. The Washington University in St. Louis Animal Studies IACUC Committee approved all experimental methods.

Viral injections and surgical procedures for fiber optic placement

All surgeries were performed under isoflurane anesthesia (Piramal Healthcare, Maharashtra, India). For slice physiology experiments, adult mice were injected bilaterally with AAV5-EF1α-DIO-opto-MOR-eYFP. For behavior experiments, adult male mice were injected unilaterally with 500 nl of AAV5-EF1α-DIO-opto-MOR-eYFP virus (WUSTL Hope Center Viral Core, St. Louis, MO) into the RMTg (AP: −3.9 mm, ML: −0.1 mm, DV: −4.5 mm) or the VP (AP: 0.7 mm, ML: 1 mm, DV: −5.25 mm. Fiber optic ferrules were chronically implanted above the VTA (AP: −3.4 mm, ML: −0.5 mm, DV: −4.0 mm) or the VP (AP: 0.7 mm, ML: 1 mm, DV: −4.8 mm) respectively and dental cement (Lang Dental, Wheeling, IL) was applied to hold the ferrules in place (Sparta et al., 2012). Mice were allowed to recover

Author Manuscript Author Manuscript Author Manuscript Author Manuscript

for at least three weeks following infusion of virus and fiber placement prior to further behavioral testing.

Slice physiology

Acute brain slices were prepared using a protective cutting and recovery method (Ting et al., 2014). Anesthetized mice were transcardially perfused with NMDG-substituted aCSF containing (in mM): 93 NMDG, 2.5 KCl, 1.25 NaH_2PO_4, 30 $NaHCO_3$, 20 HEPES, 25 glucose, 5 ascorbic acid, 2 thiourea, 3 Na-pyruvate, 12 *N*-acetyl-L-cysteine, 10 $MgSO_4$, 0.5 $CaCl_2$, pH=7.3. 200 μm thick coronal sections of the PAG were cut using a Vibratome VT1000s (Leica) and transferred to an oxygenated recovery chamber containing NMDG aCSF for 5–10 minutes at 32–34°C, before being transferred to a holding chamber filled with modified aCSF containing (in mM): 92 NaCl, 2.5 KCl, 1.2 NaH_2PO_4, 30 $NaHCO_3$, 20 HEPES, 25 glucose, 2 $CaCl_2$, 2 $MgCl_2$, pH adjusted to 7.3 with NaOH, Osm 300–315; and were incubated in the dark at room temperature for >1 hr before recording. 225 μm thick sagittal sections were prepared for experiments in RMTg. Additional details can be found in Supplemental Experimental Procedures.

Behavior

Real-time place preference and aversion (rtPP/A)—Mice were placed into a custom made black acrylic two-chambered box (52.5 × 25.5 × 25.5 cm) and allowed to explore each of two chambers for 60 minutes. Using Noldus Ethovision hardware controller connected to a master 9 functional generator, light stimulation (473 nm, 10 mW) was delivered through fiber optic implants during the duration of their time spent in the “conditioned” side of the camber and mice received no stimulation on the “unconditioned” side. The experimental animals were counterbalanced for both group and conditioning side. Preference and aversion scores in each experiment were determined by comparing the amount of time spent in the conditioned vs. unconditioned sides during the real time testing phase. Preference (RMTg) and aversion (VP) were calculated by comparing time spent in the light stimulation box with time spent in the no stimulation box during the final 30 minutes of the test session. All behavioral data (locomotion, velocity, entries) was analyzed using Noldus Ethovision (v9.5) with a ZR900 Canon camera.

Immunohistochemistry

As previously described (Kim et al., 2013), after the conclusion of behavioral testing, mice were anesthetized with sodium pentobarbital and transcardially perfused with ice cold PBS, followed by 4% phosphate-buffered paraformaldehyde. Brains were removed, post-fixed overnight in paraformaldehyde, and saturated in 30% phosphate-buffered sucrose. 50 μm sections were cut, washed in 0.3% Triton X100/5% normal goat serum in 0.1 M PBS, stained with fluorescent Nissl stain (1:400 Neurotrace, Invitrogen, Carlsbad, CA) for 1 hr, and mounted onto glass slides with Vectashield (Vector Laboratories, Burlingame, CA). VTA sections were stained with rabbit anti-tyrosine hydroxylase (1:1000, Millipore, Billerica, MA) overnight at 4°C and AlexaFluor 633 goat anti-rabbit for 2 hours at room temperature (1:1000, Molecular Probes, Eugene, OR) prior to the Nissl step. Opto-MOR expression was verified using fluorescence (Olympus, Center Valley, PA) and confocal

Author Manuscript Author Manuscript Author Manuscript Author Manuscript

microscopy (Leica Microsystems, Bannockburn, IL). Images were produced with Leica Application Suite Advanced Fluorescence software. Animals that did not show targeted expression were excluded.

Supplementary Material

Refer to Web version on PubMed Central for supplementary material.

Acknowledgments

This work is supported by EUREKA NIDA R01DA037152 (to MRB), NIMH F31MH101956 (JGM), NSTR01NS081707 (to RG, MRB), NIDA K99DA038725 (to RAH) the W.M. Keck Fellowship in Molecular Medicine (MJS, BAC) and TR32 GM108539 (BAC). MAB was supported by the Howard Hughes Medical Institute. We would like to thank Vijay Samenni and Clint Morgan in the Gereau lab for their assistance. We would also like to thank the Hope Center Viral Core at Washington University-St. Louis. We thank Skylar Spangler, Lamley Lawson and other members of the Bruchas laboratory for their help revising the manuscript and technical support. And we also thank the laboratory of Dr. Evan Kharasch for their technical support.

References

Airan RD, Thompson KR, Fenno LE, Bernstein H, Deisseroth K. Temporally precise in vivo control of intracellular signalling. Nature. 2009; 458:1025–1029. [PubMed: 19295515]

Atasoy D, Aponte Y, Su HH, Sternson SM. A FLEX switch targets Channelrhodopsin-2 to multiple cell types for imaging and long-range circuit mapping. J. Neurosci. Off. J. Soc. Neurosci. 2008; 28:7025–7030.

Banghart MR, Sabatini BL. Photoactivatable neuropeptides for spatiotemporally precise delivery of opioids in neural tissue. Neuron. 2012; 73:249–259. [PubMed: 22284180]

Barish PA, Xu Y, Li J, Sun J, Jarajapu YPR, Ogle WO. Design and functional evaluation of an optically active μ-opioid receptor. Eur. J. Pharmacol. 2013; 705:42–48. [PubMed: 23454521]

Belcheva MM, Clark AL, Haas PD, Serna JS, Hahn JW, Kiss A, Coscia CJ. Mu and kappa opioid receptors activate ERK/MAPK via different protein kinase C isoforms and secondary messengers in astrocytes. J. Biol. Chem. 2005; 280:27662–27669. [PubMed: 15944153]

Berndt A, Lee SY, Ramakrishnan C, Deisseroth K. Structure-guided transformation of channelrhodopsin into a light-activated chloride channel. Science. 2014; 344:420–424. [PubMed: 24763591]

Blanchet C, Lüscher C. Desensitization of mu-opioid receptor-evoked potassium currents: initiation at the receptor, expression at the effector. Proc. Natl. Acad. Sci. U. S. A. 2002; 99:4674–4679. [PubMed: 11917119]

Bruchas MR, Schindler AG, Shankar H, Messinger DI, Miyatake M, Land BB, Lemos JC, Hagan CE, Neumaier JF, Quintana A, et al. Selective p38α MAPK deletion in serotonergic neurons produces stress resilience in models of depression and addiction. Neuron. 2011; 71:498–511. [PubMed: 21835346]

Celver J, Xu M, Jin W, Lowe J, Chavkin C. Distinct Domains of the μ-Opioid Receptor Control Uncoupling and Internalization. Mol. Pharmacol. 2004; 65:528–537. [PubMed: 14978231]

Childers SR, Snyder SH. Guanine nucleotides differentiate agonist and antagonist interactions with opiate receptors. Life Sci. 1978; 23:759–761. [PubMed: 211364]

Gunaydin LA, Grosenick L, Finkelstein JC, Kauvar IV, Fenno LE, Adhikari A, Lammel S, Mirzabekov JJ, Airan RD, Zalocusky KA, et al. Natural Neural Projection Dynamics Underlying Social Behavior. Cell. 2014; 157:1535–1551. [PubMed: 24949967]

Gupta A, Gomes I, Wardman J, Devi LA. Opioid receptor function is regulated by post-endocytic peptide processing. J. Biol. Chem. 2014; 289:19613–19626. [PubMed: 24847082]

Al-Hasani R, Bruchas MR. Molecular mechanisms of opioid receptor-dependent signaling and behavior. Anesthesiology. 2011; 115:1363–1381. [PubMed: 22020140]

Author Manuscript Author Manuscript Author Manuscript Author Manuscript

Hille B. Modulation of ion-channel function by G-protein-coupled receptors. Trends Neurosci. 1994; 17:531–536. [PubMed: 7532338]

Hjelmstad GO, Xia Y, Margolis EB, Fields HL. Opioid Modulation of Ventral Pallidal Afferents to Ventral Tegmental Area Neurons. J. Neurosci. 2013; 33:6454–6459. [PubMed: 23575843]

Ingram SL, Macey TA, Fossum EN, Morgan MM. Tolerance to repeated morphine administration is associated with increased potency of opioid agonists. Neuropsychopharmacol. Off. Publ. Am. Coll. Neuropsychopharmacol. 2008; 33:2494–2504.

Irannejad R, Tomshine JC, Tomshine JR, Chevalier M, Mahoney JP, Steyaert J, Rasmussen SGF, Sunahara RK, El-Samad H, Huang B, et al. Conformational biosensors reveal GPCR signalling from endosomes. Nature. 2013; 495:534–538. [PubMed: 23515162]

Jalabert M, Bourdy R, Courtin J, Veinante P, Manzoni OJ, Barrot M, Georges F. Neuronal circuits underlying acute morphine action on dopamine neurons. Proc. Natl. Acad. Sci. U. S. A. 2011; 108:16446–16450. [PubMed: 21930931]

Jennings JH, Sparta DR, Stamatakis AM, Ung RL, Pleil KE, Kash TL, Stuber GD. Distinct extended amygdala circuits for divergent motivational states. Nature. 2013; 496:224–228. [PubMed: 23515155]

Jhou TC, Xu S-P, Lee MR, Gallen CL, Ikemoto S. Mapping of reinforcing and analgesic effects of the mu opioid agonist Endomorphin-1 in the ventral midbrain of the rat. Psychopharmacology (Berl.). 2012; 224:303–312. [PubMed: 22669129]

Kim J-M, Hwa J, Garriga P, Reeves PJ, RajBhandary UL, Khorana HG. Light-Driven Activation of β2-Adrenergic Receptor Signaling by a Chimeric Rhodopsin Containing the β2-Adrenergic Receptor Cytoplasmic Loops†. Biochemistry (Mosc.). 2005; 44:2284–2292.

Kim T, McCall JG, Jung YH, Huang X, Siuda ER, Li Y, Song J, Song YM, Pao HA, Kim R-H, et al. Injectable, cellular-scale optoelectronics with applications for wireless optogenetics. Science. 2013; 340:211–216. [PubMed: 23580530]

Li X, Gutierrez DV, Hanson MG, Han J, Mark MD, Chiel H, Hegemann P, Landmesser LT, Herlitze S. Fast noninvasive activation and inhibition of neural and network activity by vertebrate rhodopsin and green algae channelrhodopsin. Proc. Natl. Acad. Sci. U. S. A. 2005; 102:17816–17821. [PubMed: 16306259]

Lüscher C, Jan LY, Stoffel M, Malenka RC, Nicoll RA. G protein-coupled inwardly rectifying K+ channels (GIRKs) mediate postsynaptic but not presynaptic transmitter actions in hippocampal neurons. Neuron. 1997; 19:687–695. [PubMed: 9331358]

Masseck OA, Spoida K, Dalkara D, Maejima T, Rubelowski JM, Wallhorn L, Deneris ES, Herlitze S. Vertebrate cone opsins enable sustained and highly sensitive rapid control of Gi/o signaling in anxiety circuitry. Neuron. 2014; 81:1263–1273. [PubMed: 24656249]

Matsui A, Williams JT. Opioid-Sensitive GABA Inputs from Rostromedial Tegmental Nucleus Synapse onto Midbrain Dopamine Neurons. J. Neurosci. 2011; 31:17729–17735. [PubMed: 22131433]

Matsui A, Jarvie BC, Robinson BG, Hentges ST, Williams JT. Separate GABA Afferents to Dopamine Neurons Mediate Acute Action of Opioids, Development of Tolerance, and Expression of Withdrawal. Neuron. 2014

Raimondo JV, Kay L, Ellender TJ, Akerman CJ. Optogenetic silencing strategies differ in their effects on inhibitory synaptic transmission. Nat. Neurosci. 2012; 15:1102–1104. [PubMed: 22729174]

Roy A, Kucukural A, Zhang Y. I-TASSER: a unified platform for automated protein structure and function prediction. Nat. Protoc. 2010; 5:725–738. [PubMed: 20360767]

Da Silva S, Hasegawa H, Scott A, Zhou X, Wagner AK, Han B-X, Wang F. Proper formation of whisker barrelettes requires periphery-derived Smad4-dependent TGF-beta signaling. Proc. Natl. Acad. Sci. U. S. A. 2011; 108:3395–3400. [PubMed: 21300867]

Smith KS, Berridge KC. The ventral pallidum and hedonic reward: neurochemical maps of sucrose “liking” and food intake. J. Neurosci. Off. J. Soc. Neurosci. 2005; 25:8637–8649.

Smith KS, Tindell AJ, Aldridge JW, Berridge KC. Ventral pallidum roles in reward and motivation. Behav. Brain Res. 2009; 196:155–167. [PubMed: 18955088]

Author Manuscript Author Manuscript Author Manuscript Author Manuscript

Sparta DR, Stamatakis AM, Phillips JL, Hovelsø N, van Zessen R, Stuber GD. Construction of implantable optical fibers for long-term optogenetic manipulation of neural circuits. Nat. Protoc. 2012; 7:12–23. [PubMed: 22157972]

Tan KR, Yvon C, Turiault M, Mirzabekov JJ, Doehner J, Labouèbe G, Deisseroth K, Tye KM, Lüscher C. GABA Neurons of the VTA Drive Conditioned Place Aversion. Neuron. 2012; 73:1173–1183. [PubMed: 22445344]

Ting JT, Daigle TL, Chen Q, Feng G. Acute brain slice methods for adult and aging animals: application of targeted patch clamp analysis and optogenetics. Methods Mol. Biol. Clifton NJ. 2014; 1183:221–242.

Tsvetanova NG, von Zastrow M. Spatial encoding of cyclic AMP signaling specificity by GPCR endocytosis. Nat. Chem. Biol. 2014 advance online publication.

Vaughan CW, Bagley EE, Drew GM, Schuller A, Pintar JE, Hack SP, Christie MJ. Cellular actions of opioids on periaqueductal grey neurons from C57B16/J mice and mutant mice lacking MOR-1. Br. J. Pharmacol. 2003; 139:362–367. [PubMed: 12770941]

Vong L, Ye C, Yang Z, Choi B, Chua S Jr. Lowell BB. Leptin Action on GABAergic Neurons Prevents Obesity and Reduces Inhibitory Tone to POMC Neurons. Neuron. 2011; 71:142–154. [PubMed: 21745644]

Wietek J, Wiegert JS, Adeishvili N, Schneider F, Watanabe H, Tsunoda SP, Vogt A, Elstner M, Oertner TG, Hegemann P. Conversion of channelrhodopsin into a light-gated chloride channel. Science. 2014; 344:409–412. [PubMed: 24674867]

Van Zessen R, Phillips JL, Budygin EA, Stuber GD. Activation of VTA GABA Neurons Disrupts Reward Consumption. Neuron. 2012; 73:1184–1194. [PubMed: 22445345]

Zhang F, Gradinaru V, Adamantidis AR, Durand R, Airan RD, de Lecea L, Deisseroth K. Optogenetic interrogation of neural circuits: technology for probing mammalian brain structures. Nat. Protoc. 2010; 5:439–456. [PubMed: 20203662]

Zhou X, Wang L, Hasegawa H, Amin P, Han B-X, Kaneko S, He Y, Wang F. Deletion of PIK3C3/Vps34 in sensory neurons causes rapid neurodegeneration by disrupting the endosomal but not the autophagic pathway. Proc. Natl. Acad. Sci. U. S. A. 2010; 107:9424–9429. [PubMed: 20439739]

Author Manuscript Author Manuscript Author Manuscript Author Manuscript

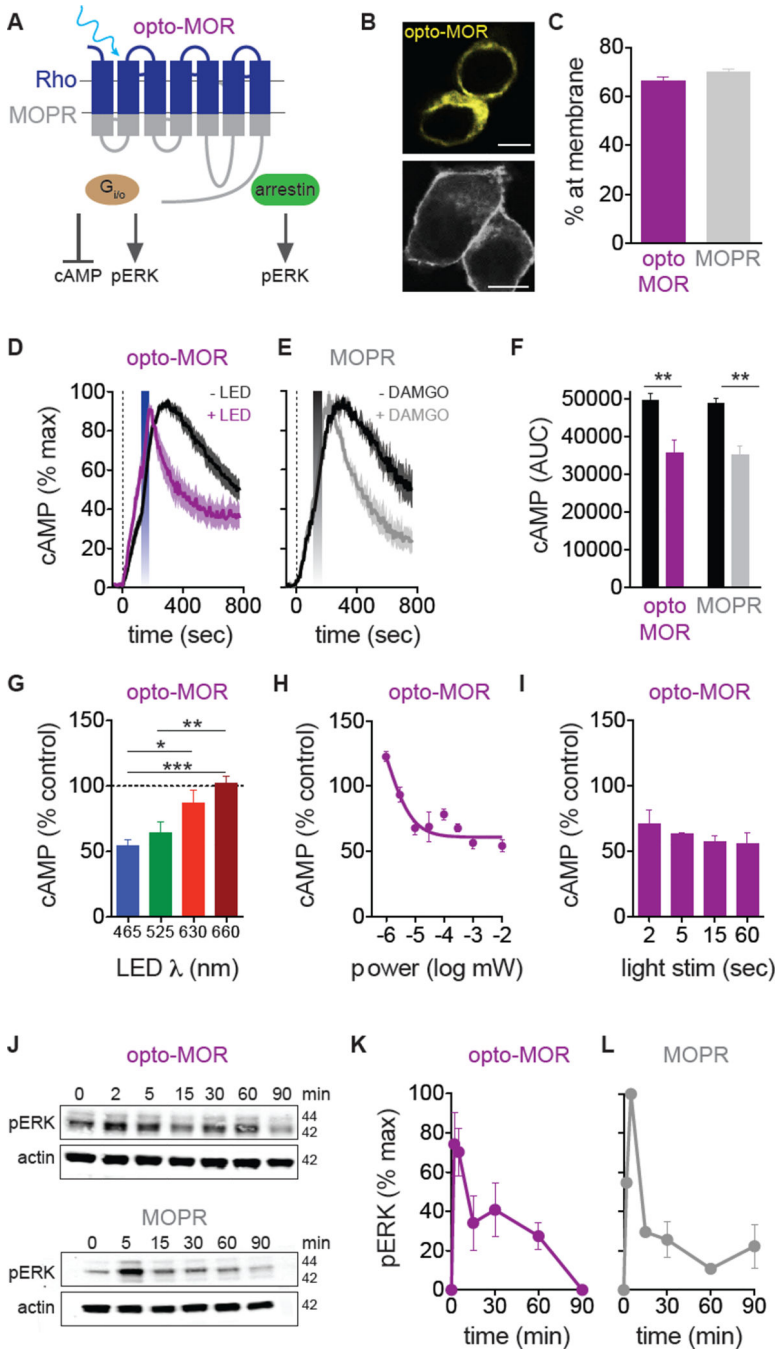

Figure 1. Opto-MOR and MOR share canonical intracellular G-protein signaling mechanisms

(A) Schematic of opto-MOR showing activation of cAMP and pERK pathways. **(B)** Opto-MOR and MOPR are highly expressed at membrane in HEK293 cells (scale bar = 10 μm). **(C)** Opto-MOR (purple n = 43 cells) and MOPR (n = 37 cells) share similar surface expression in HEK293 cells. **(D)** Optical stimulation (blue bar; 20 sec, 1 mW) of opto-MOR reduces forskolin-induced (dashed line) cAMP in HEK cells (n = 9–10 experiments). **(E)** Application of DAMGO (grey bar; 1 μM) reduces forskolin-induced (dashed line) cAMP in HEK293 cells expressing MOPR (n = 3 experiments). **(F)** Light and DAMGO significantly

Author Manuscript Author Manuscript Author Manuscript Author Manuscript

reduce forskolin-induced cAMP in opto-MOR (purple; n = 12) and MOPR (grey; n = 3). **(G)** cAMP inhibition by opto-MOR is most efficient at 465 nm (n = 6–8 experiments; * $p < 0.05$, ** $p < 0.01$; *** $p < 0.001$ via One-Way ANOVA with Bonferroni's Multiple Comparison Test). **(H)** cAMP inhibition by opto-MOR is not dependent on light pulse length (n = 2–10 experiments). **(I)** cAMP inhibition by opto-MOR is power dependent (n = 3–9 experiments). **(J)** Representative immunoblots show similar kinetic increases in pERK in response to light (1 min, 1 mW) or DAMGO (1 μM) in opto-MOR (purple) and MOPR (grey) expressing cells. **(F)** Quantification of light-induced pERK in opto-MOR (n = 6) and **(L)** DAMGO-induced pERK in MOPR (n = 2). Data are represented as mean ± SEM. See also Figures S1 and S2.

Author Manuscript Author Manuscript Author Manuscript Author Manuscript

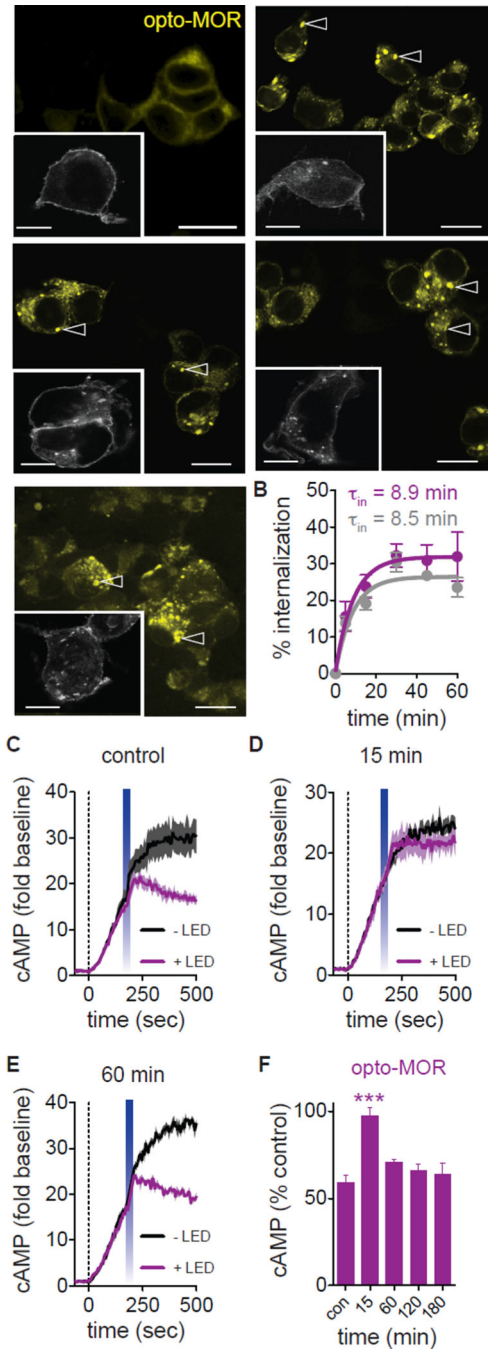

Figure 2. Opto-MOR and MOPR internalization and recovery from desensitization

(A) Representative images show internalization of opto-MOR (colorized yellow; scale bar = 50 μm) and MOPR (inset; grey; scale bar = 10 μm) expressed in HEK293 cells in response to light and DAMGO. 0, 5, 15, 30 and 45 min time points represented. Arrowheads show examples of internalized receptor. **(B)** Quantification of receptor internalization in opto-MOR (purple; τ_{in} = 8.9 min; n = 16–43 cells per time point over 2 experimental replicates) and MOPR (grey; τ_{in} = 8.5 min; n = 24–38 cells per time point over 3 experimental replicates) in response to light and DAMGO-induced activation respectively. **(C)** Opto-

Author Manuscript Author Manuscript Author Manuscript Author Manuscript

MOR inhibits forskolin-induced (dashed line) cAMP following light stimulation (n = 4 traces). **(D)** A second light pulse 15 min following the first shows a loss of opto-MOR activity (n = 3–4 traces). **(E)** cAMP inhibitory activity returns to baseline levels 60 min following an initial light pulse (n = 3 traces). **(F)** Time course of recovery from desensitization (n = 3–11 replicates; *** $p < 0.001$ via One Way ANOVA followed by Dunnett's Multiple Comparison Test to control). Data are represented as mean ± SEM. See also Figure S2.

Author Manuscript Author Manuscript Author Manuscript Author Manuscript

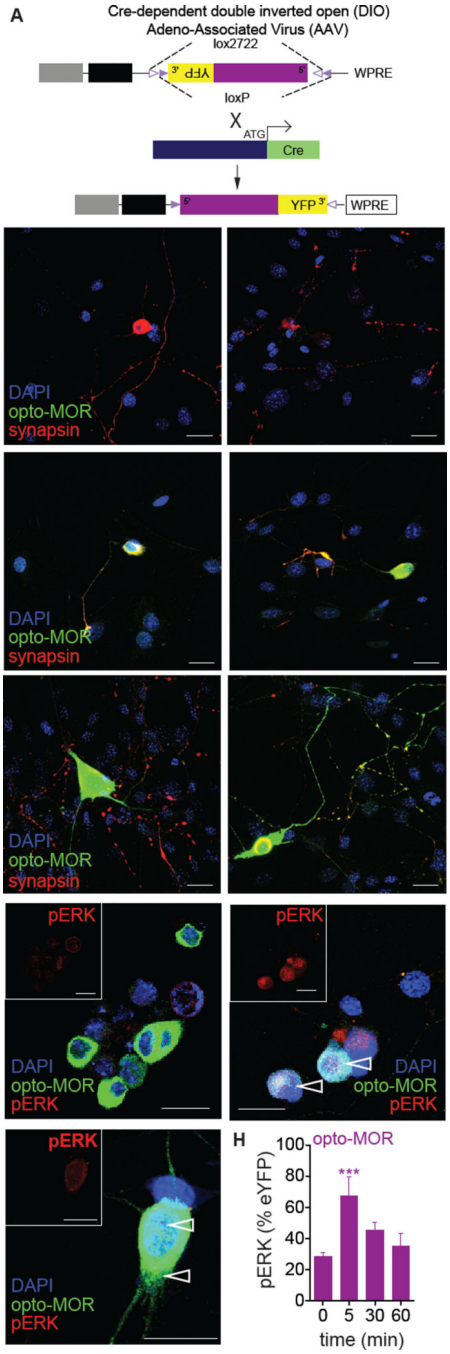

Figure 3. Opto-MOR expression and function in DRG neurons

(A) Opto-MOR packaged into an AAV5-DIO, EF1α-YFP viral construct. Cre expression is driven from the sensory neuron-specific Advillin promoter following insertion after the initial start codon, resulting in Cre-mediated recombination and inversion of the opto-MOR construct into the appropriate 5'–3' orientation. **(B)** Uninfected DRGs colabeled with the nuclear stain DAPI (blue) and synapsin (red). **(C)** Opto-MOR expression (green) in DRGs 2 days *in vitro* (DIV). Large arrowheads point to the soma of infected neurons. **(D)** Opto-MOR expression (green) in DRGs 5 DIV. Small arrowheads highlight opto-MOR

Author Manuscript Author Manuscript Author Manuscript Author Manuscript

expression in synaptic terminals colabeled with synapsin (red). Scale bars for panels B-D = 30 μm. **(E)** Unstimulated opto-MOR expressed in DRGs after 5 DIV labeled with pERK (red; and inset). **(F)** Opto-MOR expressing DRGs (5 DIV) 5 min following photostimulation and labeled for pERK (red; and inset). Open arrows denote internalized punctate receptors. **(G)** Higher magnification of opto-MOR expressing DRGs (5 DIV) 5 min following photostimulation and labeled for pERK (red; and inset). Open arrows denote internalized punctate receptors. **(H)** pERK intensity normalized to opto-MOR-YFP intensity at varying times following photostimulation (n = 3–32 DRG neurons per time point; *** $p < 0.001$ via One Way ANOVA followed by Dunnett's Multiple Comparison Test to 0 min. Scale bars for panels E-G = 20 μm. Data are represented as mean ± SEM.

Author Manuscript Author Manuscript Author Manuscript Author Manuscript

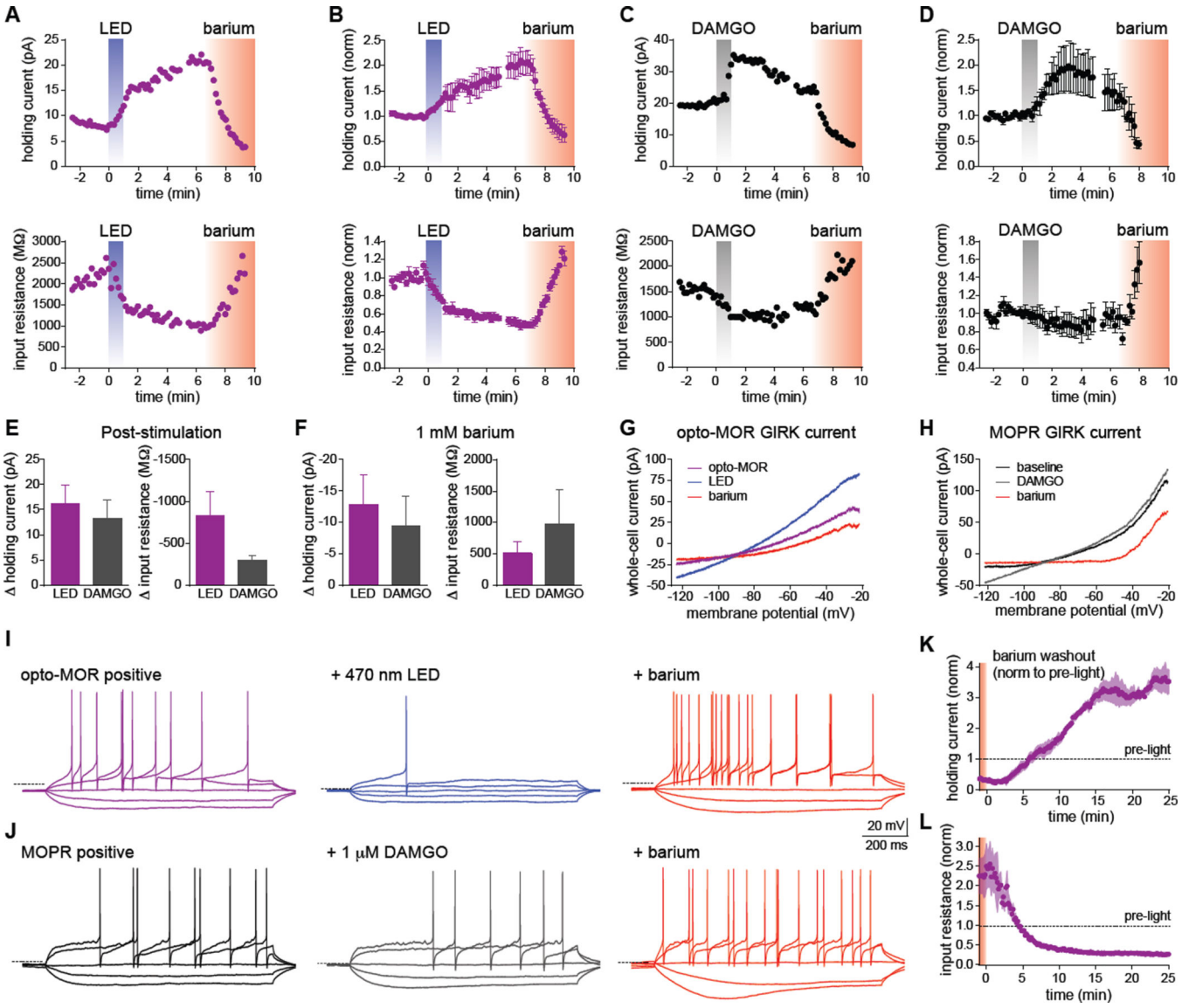

Figure 4. Photostimulation of opto-MOR and activation of endogenous MOPRs have similar effects on neuronal physiology and excitability in GABAergic PAG neurons

(A) Representative plots from an opto-MOR$^+$ neuron in acute PAG slices illuminated with 470 nm LED light (10 mW/mm^2) for 60s. The top trace shows a rapid outward current in response to illumination, while the bottom trace depicts the simultaneous drop in input resistance. Bath application of 1 mM barium (red shading) blocked both the outward current and reversed the change in input resistance. **(B)** Normalized summary plots showing the response to LED stimulation from additional opto-MOR$^+$ neurons as described in panel A (n=4). **(C)** Example traces recorded from a MOPR$^+$ neuron stimulated with 1 μM DAMGO (grey bars) showing similar outward currents (top) and decreased input resistance (bottom) compared to opto-MOR$^+$ neurons shown in panels A and B. **(D)** Normalized summary plots from additional MOPR$^+$ neurons depicting the response to DAMGO as described in panel C (n=4). **(E)** Quantification of the peak changes in holding current and input resistance following LED (purple) or DAMGO (gray) stimulation (n=4). **(F)** Quantification of the peak

Author Manuscript Author Manuscript Author Manuscript Author Manuscript

changes in holding current and input resistance after application of 1 mM barium (n=4). **(G–H)** Representative current-voltage traces from a 250 ms voltage ramp from −20 to −120 mV, in an opto-MOR$^+$ neuron before (purple trace) and after 60s LED stimulation (blue), or a MOPR$^+$ neuron before (black) or after stimulation with 1 μM DAMGO (gray). Both currents were reduced by the GIRK channel blocker barium (1 mM, red). (I–J) Left traces depict voltage traces from current-clamp recordings of an opto-MOR$^+$ (purple traces) or MOPR$^+$ neuron (black) in response to hyperpolarizing current injections of −20 and −10 pA, and depolarizing current injections of 1- and 2-times rheobase. Middle traces show decreased input resistance and excitability following LED (blue) and DAMGO (gray), in response to the same current injections before stimulation. The right traces demonstrate the increased input resistance and neuronal excitability observed following GIRK channel block with 1 mM barium (red). Dashed lines indicate −60 mV membrane potential. **(K–L)** Normalized summary plots of the persistent outward current (K) and decreased input resistance **(L)** in opto-MOR$^+$ neurons following light stimulation and subsequent barium washout (n=3). These effects were observed >45 min after 60s LED stimulation. The dashed lines indicate the average response before illumination. Data are represented as mean ± SEM. See also Figure S4.

Author Manuscript Author Manuscript Author Manuscript Author Manuscript

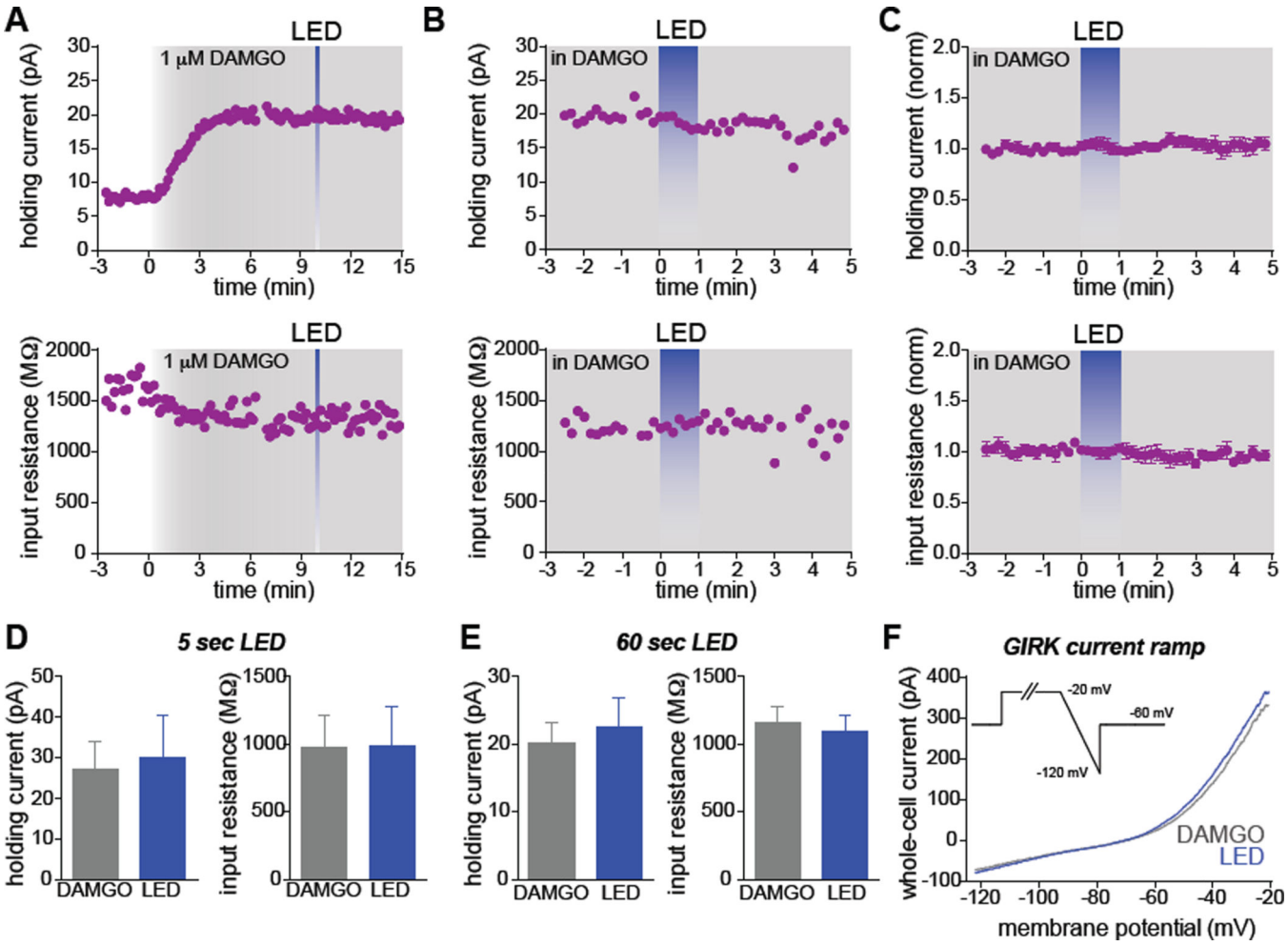

Figure 5. Activation of endogenous mu opioid receptors occludes GIRK channel activation by opto-MORs

(A) Example plots from an opto-MOR and MOPR^{+} GABAergic neuron in the PAG. An outward current and simultaneous decrease in input resistance were observed following prolonged application of 1 μM DAMGO, which plateaued after ~5 min. Brief (5s) LED illumination did not result in further changes to either of these parameters. **(B)** Example plots from a different neuron positive for both opto-MOR and MOPR in the presence of 1 μM DAMGO. The plateaued response to DAMGO is not shown in this example. Prolonged LED illumination (blue, 60s) did not alter the holding current or input resistance. **(C)** Normalized summary graph showing the occluded responses to LED illumination following stimulation of endogenous MOPRs with DAMGO (n=3). **(D)** Quantification of the holding current and input resistance in the presence of DAMGO and following 5s of LED stimulation (n=3). **(E)** Same quantification as in panel D, but with 60s illumination (n=3). **(F)** Representative GIRK channel ramp in the presence of DAMGO and following LED stimulation. Data are represented as mean ± SEM.

Author Manuscript Author Manuscript Author Manuscript Author Manuscript

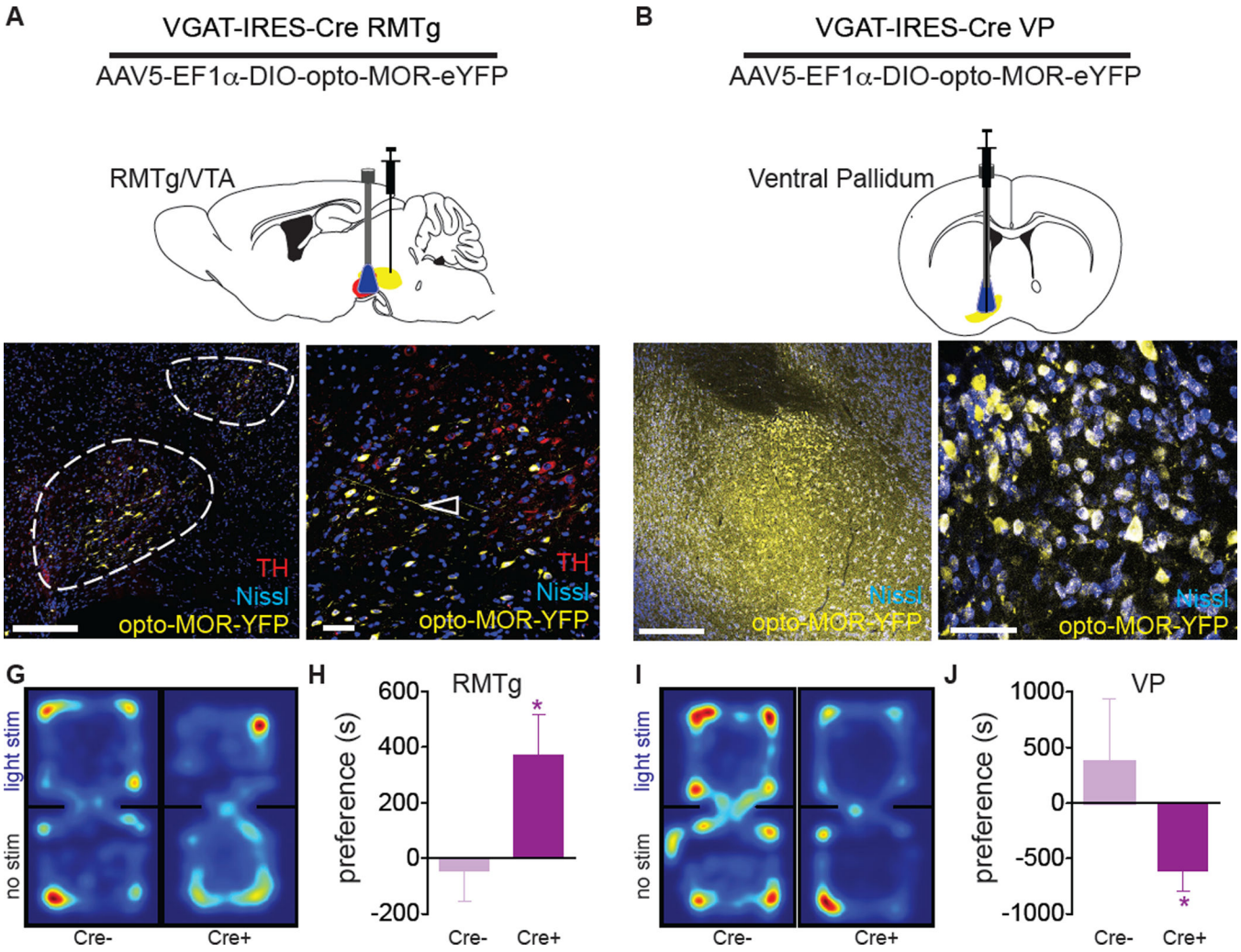

Figure 6. Photostimulation of opto-MOR causes MOR-like behavioral profiles *in vivo*

(A) Mice with AAV5-DIO-opto-MOR-YFP injected into the RMTg (yellow) with a fiber optic implanted into the VTA (red) and **(B)** the ventral pallidum. **(C,D)** Viral expression in fibers (open arrows) projecting into the VTA (identified by tyrosine hydroxylase staining in red) as well as GABAergic interneurons of the VTA (closed arrows). **(E,F)** Viral expression in VP GABA neurons (open arrows). Mice expressing opto-MOR in the RMTg-VTA (n=8) display significantly increased real-time preference behavior compared to controls (Cre- littermates, n=7) as shown by representative position heat maps **(G)** and the mean preference for the stimulation-paired chamber **(H). (I)** Mice injected into the VP (n=16) display the converse aversion behavior in the place preference assay compared to controls (Cre- littermate controls, n=5) spending less time in the light stimulated chamber also shown by position heat maps **(I)** and mean place preference results **(J)**. *p<0.05 via unpaired t-test. Data are represented as mean ± SEM. See also Figure S5.